Phase-Specific Characteristics of Wintertime Clouds across a Midlatitude Mountain Range

S. W. DORSI, M. D. SHUPE, P. O. G. PERSSON, AND D. E. KINGSMILL

Cooperative Institute for Research in Environmental Sciences, University of Colorado Boulder, and NOAA/Earth System Research Laboratory, Boulder, Colorado

L. M. AVALLONE*

Laboratory for Atmospheric and Space Physics, University of Colorado Boulder, Boulder, Colorado

(Manuscript received 5 April 2015, in final form 17 June 2015)

ABSTRACT

Observations from a series of frontal and postfrontal storms during the Colorado Airborne Multiphase Cloud Study (CAMPS) are combined to show transitions in cloud dynamics and microphysical statistics over a mountain range. During 10 flights in 2010 and 2011, along-wind, across-ridge transects over the Colorado Park Range are performed to statistically characterize air motion and microphysical conditions and their variability. Composite transect statistics show median vertical winds to be mostly upward windward of the ridge axis, and that cloud water concentration (CWC) and ice-particle number concentration are greatest near the ridge. Mixed-phase clouds were found throughout the study area, but increase in frequency by 70% relative to other cloud types in the vicinity of the range. Compared to ice-only clouds, mixed-phase clouds are associated with greater near-ridge increases in CWC and preferentially occur in regions with greater vertical wind variability or updrafts. Strong leeside reductions in CWC, the abundance of mixed-phase clouds, and number concentration of ice particles reflect the dominance of precipitation and particle mass loss processes, rather than cloud growth processes, downwind from the topographic barrier. On days in which the air column stability does not support lee subsidence, this spatial configuration is markedly different, with both ice- and liquid-water-bearing clouds appearing near the ridgeline and extending downwind. A case study from 9 January 2011 highlights mixed-phase regions in trapped lee waves, and in a near-ridgetop layer with evidence of low-altitude ice particle growth.

1. Introduction

The phase of cloud water has important impacts on cloud radiative properties, cloud lifetime, and the formation of precipitation. Mixed-phase clouds—those in which liquid droplets and ice particles coexist—are of special interest for their role on precipitation processes, for their impact on global energy budgets (Gregory and Morris 1996), and for the continuing challenges encountered in their microphysical representation in numerical models (Klein et al. 2009). The importance of mixed-phase clouds is particularly significant in mountainous regions, where mixed-phase cloud processes may influence both the locations that experience precipitation (Reinking and Snider 2000) and the total water mass that precipitates (Lowenthal et al. 2011; Saleeby et al. 2009).

Because of the difficulty of retrieving mixed-phase cloud properties using remote sensing observations (Shupe et al. 2008) and the limitations of line-of-sight measurements in complex terrain, many studies of mountain-region mixed-phase clouds have relied upon airborne in situ measurements. These airborne studies have yielded important insights into the linkages between topography, supercooled liquid water, and precipitation processes. Rauber (1992) showed evidence of riming and secondary ice production over the California Sierra Nevada and concluded that the terrain-relative

* Current affiliation: National Science Foundation, Arlington, Virginia.

Corresponding author address: S. W. Dorsi, Cooperative Institute for Research in Environmental Sciences, University of Colorado Boulder, 216 UCB, Boulder, CO 80309-0216.
E-mail: samuel.dorsi@colorado.edu

DOI: 10.1175/MWR-D-15-0135.1

location of supercooled liquid water had a strong influence on snowfall distribution. Geerts et al. (2011) suggested that snow growth mechanisms (riming, aggregation, or deposition) may operate efficiently at the intersection of the turbulent boundary layer and the lifting condensation level and so contribute strongly to low-level liquid-related snow growth. While supercooled liquid water occurs without orographic forcing in frontal systems and in Arctic stratus clouds, it is particularly common over windward mountain slopes. In the southern Rockies, in situ observations showed multiple liquid-water regions to exist above the slopes upwind from Elk Mountain (Rogers and Vali 1987), and microwave radiometer observations showed LWC to be greatest directly above the mountain slopes of the Park Range for prefrontal and frontal winter clouds (Rauber et al. 1986). The distribution of supercooled liquid water, and the resulting impacts on precipitation patterns, is influenced by the interaction of the air mass with underlying topography. However, consistent linkages between the vertical motion and precipitation fields is not always observed, as demonstrated by Kingsmill et al. (2015, manuscript submitted to *Quart. J. Roy. Meteor. Soc.*, hereafter KPHS).

The impact of liquid water in a mixed-phase cloud can depend on its vertical distribution. Liquid layers are often observed either at cloud top above precipitating ice (Fleishauer et al. 2002; Carey et al. 2008; Hogan et al. 2003b), or near cloud base below ice clouds (Rauber and Grant 1986; Heggli and Rauber 1988). For the former, these cloud-top layers can both act as source regions for ice crystal formation and growth (''generating cells''; Hobbs et al. 1980; Hogan et al. 2002), and increase net radiative cooling to space (Hogan et al. 2003a). For the latter, cloud-base liquid layers can greatly impact precipitation growth via the ''seeder-feeder mechanism'' through riming (Reinking and Snider 2000; Lowenthal et al. 2011) or deposition (Bergeron 1949). Based on a sequence of research flights over the Park Range, Rauber and Grant (1986) highlighted three regions of wintertime clouds in which liquid water tends to appear: at cloud top, where ice particle concentrations are low due to the fallout of large crystals; at cloud base, where slow crystal growth rates and rapid condensate production rates exist; and at those locations where strong orographic lift occurs, and thus condensate supply is very high. The vertical distribution of liquid and ice water may depend more on cloud type and less on temperature (Noh et al. 2013), with low-based, synoptically forced snow-producing clouds (e.g., nimbostratus) having relatively more liquid water near cloud base and midlevel clouds (e.g., altocumulus and altostratus) having more liquid water at cloud top.

Many of these observational studies rely on airborne campaigns encompassing single flights or brief sequences of flights, or focus on regions with little topographic relief. Thus, an important question remains regarding the generality of these results for different synoptic conditions and mountain environments. The current study presents a microphysical characterization of storms observed above the Park Range in Colorado during the course of 10 flights over three months. While the spatial distribution of cloud water at any time is strongly dependent on frontal forcing and the synoptic environment, the observations from these flights, encompassing various flow regimes and synoptic conditions, show the broader seasonal situation over the range. Statistical composites from the flights are used to characterize the storm structure relative to the mountain range, with a particular focus on the distribution of, and processes related to, cloud water and precipitation formation. As a means to provide context for the statistics-composite analysis, a case study from a single flight is also presented to highlight specific impacts of the topographic barrier on mixed-phase cloud processes.

2. Campaign and site description

The Colorado Airborne Multiphase Cloud Study (CAMPS) was conducted to investigate the impacts of complex topography on winter storms at a midlatitude site. Flight operations for the campaign were conducted with the University of Wyoming King Air (UWKA), a Beechcraft Super King Air 200T aircraft modified for atmospheric research (e.g., Wang et al. 2012) and equipped with a range of in situ and remote sensors. Flights were performed from 15 December 2010 through 28 February 2011, and were based at the University of Wyoming hangar in Laramie, Wyoming. During the campaign, 29 research flights were made over the mountains of southern Wyoming and the Park Range of northern Colorado (Fig. 1); data from 10 of these flights are presented in this study.

The Park Range was targeted for this project for its largely unobstructed western fetch and pronounced topographic relief, the frequent wintertime mixed-phase clouds observed in the region (e.g., Hindman 1986; Rauber et al. 1986), and the availability of complementary ground-based resources at Storm Peak Laboratory (SPL). SPL is a permanent atmospheric research facility (Borys and Wetzel 1997) located on the west summit of Mount Werner (3220 m MSL) in the Park Range above Steamboat Springs, Colorado. Ground-based observations and balloon-borne soundings were made from a site on the floor of the Yampa River valley (2078 m MSL) located 11 km west of the Park Range

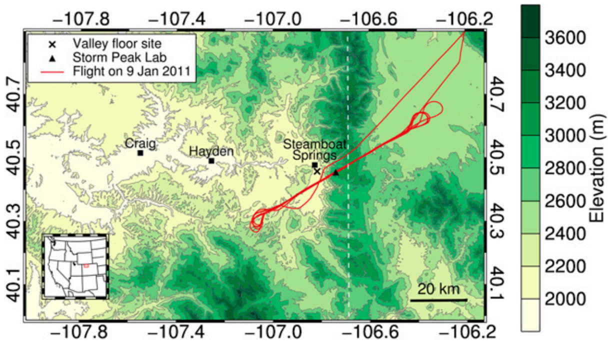

FIG. 1. Topographic map of the Park Range and vicinity, including flight track from UWKA operations on 9 Jan 2011.

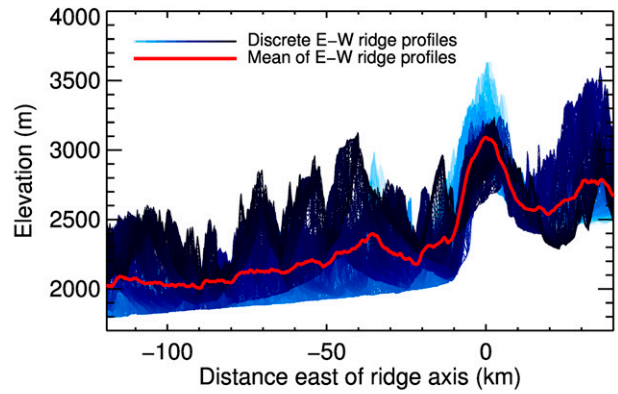

FIG. 2. East–west topographic profiles over Park Range study area, including discrete profiles at 4-arc-s intervals and the meridional mean elevation. The discrete profiles, which reflect the terrain at distinct latitudes, are plotted with a range of blue colors to facilitate their differentiation. The horizontal distance scale is relative to the ridge axis, as determined by the location of the maximum in meridional mean surface elevation.

ridge axis and 6.2 km from SPL. This ''valley floor site'' was operated as part of the Storm Peak Laboratory Cloud Property Validation Experiment (StormVEx), sponsored by the U.S. Department of Energy's Atmospheric Radiation Measurement Program, which took place over the same time period as CAMPS.

The Park Range is located along a north–south line oriented roughly orthogonal to the predominant westerly winds (Hallar et al. 2011). West of the range is the town of Steamboat Springs, the Yampa River valley, and some lower mountains and ridges. At 65 km to the southwest is the Flattop Range and to the northwest is Elk Mountain, both major topographic barriers. To the east are the Rabbit Ears Range and North Park basin. The Park Range is a primary orographic barrier for synoptic cyclones arriving from the west, and the area experiences a greater frequency of liquid-water clouds at the surface than is found at comparable elevation ranges in central Colorado (Hindman 1986; Saleeby et al. 2011). East–west (E–W) transects across the study area and its western fetch show the ridgeline of the Park Range rising 600–1500 m (Fig. 2). We define a horizontal distance scale relative to the location of the maximum meridional-mean elevation in the study area at 106.69°W longitude.

3. Methods

The suite of in situ cloud microphysical and remote sensing instruments carried on the UWKA is described by Wang et al. (2012). The Wyoming Cloud radar (WCR) and Wyoming Cloud lidar (WCL; Wang et al. 2009) provided spatial context for the in situ measurements. In addition, the UWKA was equipped with the University of Colorado closed-path tunable-diode laser hygrometer (CLH; Davis et al. 2007). Designed with an evaporative inlet, the CLH can be used to determine the in situ condensed water content (CWC), or the mass concentration of liquid water plus ice water (Dorsi et al. 2014). Processing of CLH observations follows Davis et al. (2007), and data affected by inlet icing were filtered manually. Measurements of LWC were made with the Particle Volume Monitor (PVM-100; Gerber et al. 1999) and the LWC-100 hotwire sensor (King et al. 1978), which rapidly sheds and produces little signal from ice particles. Two forward-scattering probes, capable of measuring particle size distributions (PSD) $\sim 3 < D < \sim 50\,\mu$m were deployed on the aircraft: the Forward Scattering Spectrometer Probe (FSSP; Baumgardner 1983) and the Cloud Droplet Probe (CDP; Lance et al. 2010). Optical array probes OAP-2DC and OAP-2DP (Gordon and Marwitz 1984) recorded 2D shadows of particles sized from 25 to 2500 μm, and from 200 to 10 000 μm, respectively, and the OAP-CIP recorded particle shadows from 25 to 2500 μm (Baumgardner et al. 2001). A Rosemount Icing Detector (RID; Baumgardner and Rodi 1989) was used to identify the presence of supercooled liquid water and has little sensitivity to ice (Cober et al. 2001). In situ observations were collected at a 1-s interval and were smoothed with a 3-s moving window.

In the PSD observations made with optical cloud probes, the smallest size bin is excluded from analysis because of increased particle sizing and counting uncertainty at these sizes (Korolev et al. 1998). Additionally, particle shattering on probe inlets may be an important issue for these measurements (e.g., Korolev et al. 2011). While algorithms have been demonstrated for the removal of shattering artifacts based on particle interarrival times, Korolev et al. (2011) found that such filtering fails to remove all shattering products, and may instead result in the rejection of natural particles. In this study, basic artifact rejection for streaking or coincident particles (Gordon and Marwitz 1984) is performed on the optical particle observations; further corrections for the presence of shattering artifacts are not made. As a result, the particle size distributions are assumed to contain both natural and shattering-produced particles, and are interpreted accordingly. The shattered crystal artifacts tend to impact size bins in the range 10–50 μm (Lawson 2011) or less than 500 μm (Korolev et al. 2011).

Vertical wind measurements are from the standard high-pass-filtered UWKA product, derived using the ''drift method,'' in which the ground velocity vector for aircraft motion is subtracted from aircraft pitot observations of the wind field. The resulting values, which reflect the local wind field, are high-pass filtered to mitigate long-term drift and bias in the inertial navigation system. The vertical wind error is estimated to be $0.08\,\mathrm{m\,s^{-1}}$, based on the mean standard deviation between vertical wind measurements made on the King Air and comparison aircraft in 1985 (Lenschow et al. 1991).

A statistical assessment is performed on the variability and distribution of measured vertical winds, CWC, and other parameters; this analysis combines data from transects at multiple times and locations along the mountain range. Data are organized into bins as a function of ridge-relative E–W distance, and statistical parameters are calculated for each bin. The bin width and number of 1-Hz observations in each bin varies by analysis and is shown in the results. Mean surface topography is also plotted as a function of ridge-relative distance; these data were extracted from the USGS digital elevation model database (Gesch 2007).

a. Methods: Air column stability

To explain the observed vertical air motion and associated cloud microphysical structure, a classical analysis of the air column stability and mountain wave tendency was performed following Durran (1990) using radiosonde profiles at the upwind valley floor site. The wave propagation and trapping characteristics of an air mass passing over a barrier can be assessed based on the vertical profile of wind speeds and the Brunt–Väisälä frequency N, or the natural frequency of air parcel buoyancy oscillations in a given stability environment. Vertical wave propagation is supported when the wave frequency is less than the Brunt–Väisälä frequency; that is, when $kU < N$, where k is the wavenumber of the terrain feature perturbing the flow and U is the horizontal wind speed. The vertical profile of the Scorer parameter l is computed as

$$l^2 = \frac{N^2}{U^2} - \frac{1}{U}\frac{\partial^2 U}{\partial z^2}, \tag{1}$$

where z is a height coordinate. Large decreases in l with height can signal that conditions for wave trapping are satisfied. A necessary condition for wave trapping in a two-layer system is

$$l_L^2 - l_U^2 > \frac{\pi^2}{4H^2}, \tag{2}$$

where l_L and l_U are the Scorer parameters for the lower and upper layers, respectively, and H is the thickness of the lower layer. Resonant lee waves in this system are permitted where $l_L > k > l_U$.

b. Methods: Cloud water phase

Cloud water phase is identified through a sequence of tests based on observations at a 1-s interval from several different cloud probes, after smoothing with a 3-s boxcar average. With variations in aircraft speed and the effect of smoothing, the resulting phase classification has a spatial resolution of ~100 m. Segments may contain phase heterogeneities at smaller spatial scales (e.g., Korolev and Isaac 2006), but such smaller scales are not considered here.

The phase-determination method is based on approaches presented in Field et al. (2004) and McFarquhar et al. (2007). First, cloud regions are identified by CWC greater than $0.005\,\mathrm{g\,m^{-3}}$, as observed with the CLH. This value is 2 times the standard deviation of the CLH CWC measurements in clear-sky conditions: where no particles are reported by the optical cloud probes. Separate consideration is also given to the phase-specific properties of dense clouds, using a threshold of $0.1\,\mathrm{g\,m^{-3}}$. Next, liquid water is identified where observations with the RID exhibit a voltage rate of $2\,\mathrm{mV\,s^{-1}}$ or greater (Cober et al. 2001). The RID undergoes periodic heating and cooling cycles to remove rime accumulation; as suggested by Korolev and Isaac (2006), phase is manually assessed during these brief periods based on hotwire LWC measurements and the FSSP- and CDP-observed small-particle concentrations. Finally, because ice particles are expected to grow rapidly to large sizes in saturated conditions, mixed-phase clouds are differentiated from liquid-only clouds by the presence of large particles. To satisfy the test for the presence of ice, the concentration of particles with $D >$ 100 μm observed with cloud probes must be greater than the estimated detection thresholds of $0.012\,\mathrm{L^{-1}}$ for the CIP and 2D-C and $0.004\,\mathrm{L^{-1}}$ for the 2D-P. Very large liquid-water particles, such as drizzle drops (Field et al. 2004; Rosenfeld et al. 2013), may be misidentified as ice because of this size criterion, and it is possible that some liquid-only drizzle-bearing clouds are classified here as mixed phase. Alternately, mixed-phase clouds in which the ice particles are exclusively smaller than 100 μm

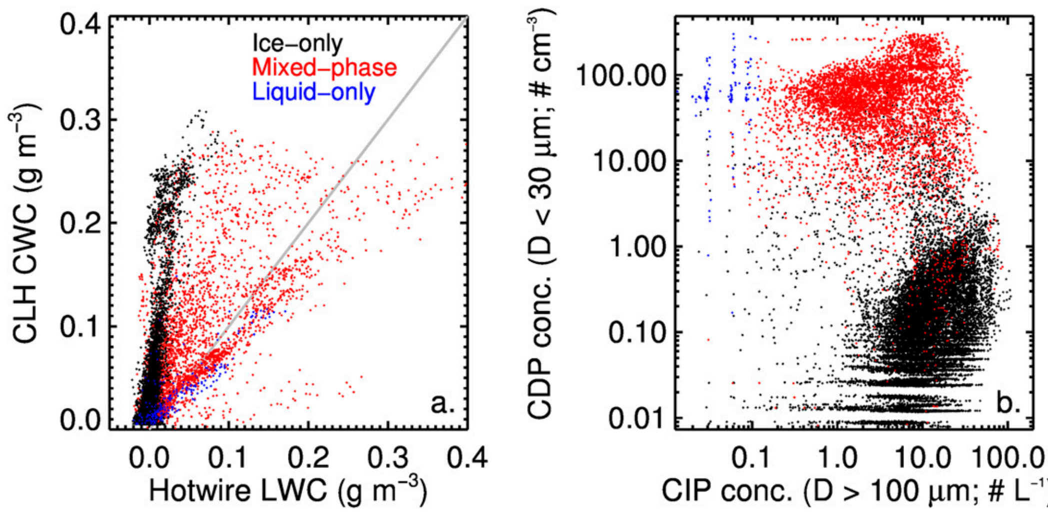

FIG. 3. For observations from each water phase group: (a) the CWC measured with CLH compared with LWC measured with DMT-100 hotwire sensor and (b) the compared number concentrations of small particles and large particles, where small particles are those counted by the CDP with $D < 30\,\mu$m and large particles are those measured by the CIP with $D > 100\,\mu$m. Points are colored by phase using the scheme labeled in the left panel.

(e.g., Cotton et al. 2010; McFarquhar et al. 2013) may be misidentified as liquid only using this algorithm; however, only 1.2% of in-cloud observations in the study were ultimately identified as liquid only, suggesting that this latter error occurs infrequently, if at all.

The efficacy of this phase-determination algorithm is demonstrated by a comparison between the hotwire LWC and CLH CWC, in which observations with these instruments (Fig. 3a) generally fall into distinct groupings by phase. In ice clouds, the hot-wire sensor reports near-zero LWC over a range of CLH-measured CWCs. Liquid-only clouds are the least prevalent in the CAMPS observations; for these clouds the hotwire sensor and CLH are expected to have an equal response and resulting observations should fall along a 1:1 line. A linear least squares fit to the liquid-only observations has a CWC–LWC slope of 0.78 ± 0.25 ($n = 358$). Because by definition CWC $\geq$ LWC, this slope likely reflects a systematic bias between these instruments, rather than a misidentification of cloud water phase. During CAMPS, the CWC observations from the CLH and the LWC from other probes correlate well within liquid-dominated regions, although the CLH reports consistently lesser values. This bias may result from incomplete vaporization of sampled hydrometeors in the CLH inlet, or overestimation of the particle sampling efficiency (Davis et al. 2007). For these reasons, the CLH CWC values presented here likely reflect a lower limit for CWC. For the CWC–LWC relationship in mixed-phase clouds the hotwire sensor and CLH should both respond to the liquid content in the cloud, while the CLH should additionally respond to the cloud ice water content (IWC). In Fig. 3a, this expected behavior is indeed reflected by the mixed-phase observations having CWC–LWC ratios between those for the ice-only and liquid-only limiting cases.

The relative abundance of small particles ($D < 30\,\mu$m) and large particles ($D > 100\,\mu$m) also differs by phase (Fig. 3b), based on observations with the CDP and CIP, respectively. Linear streaking in the plotted points results from the discretized nature of measuring particle number concentration by counting particles observed in a finite volume. Points are clustered into groups that largely coincide with identified cloud water phases. The distribution of small-particle number concentrations is bimodal, with the low number–concentration mode dominated by ice-only observations, and the high number–concentration mode dominated by liquid-only and mixed-phase observations. By design of the phase-identification algorithm, among observations where small particles are abundant, low concentrations of large particles are associated with liquid-only clouds. Because time steps are classified as mixed phase if large particles are observed by any of the CIP, 2D-C, or 2D-P, some of the observations with low CIP large-particle number concentration are classified as mixed phase. On the basis of these tests, the phase-determination approach appears to be effective in distinguishing observations by phase in most cases.

4. Case study: 9 January 2011

While much of this analysis focuses on exploring wintertime storms in a statistical manner, a more detailed case study is first presented for the flight on 9 January 2011. By highlighting specific features and processes observed in the flight transects from a single day, this case study provides context for the multiday statistical composites that are presented later, and demonstrates characteristics of the measurements used in the study. Furthermore, this case study approach has the benefit of preserving some process signatures otherwise lost to averaging, such as details about the location of liquid layers.

The UWKA flight operations on 9 January consisted of nine repeat passes along a single linear ground track over the Park Range at a fixed elevation of 4200 m [all heights are above mean sea level (MSL)], with observations collected over the period from 2131 to 2327 UTC. These observations took place in a stable air mass after the passage of a cold front. The synoptic environment over the western United States was dominated by a closed low pressure center located over central Montana (Fig. 4). A cold front passed over the Park Range study site at 1400–1500 UTC, roughly 7 h before flight operations in the area began, then remained stalled over central Colorado to the southeast of the study area until 3.5 h after the completion of flight observations (0300 UTC 10 January). The resulting winds in northern Colorado were from the west-southwest, a direction favorable for orographic ascent over the Park Range (Saleeby and Cotton 2005).

Data from radiosondes released from the valley floor site at 1743 and 2155 UTC 9 January, and 0108 UTC 10 January (Fig. 5), indicated the air column above 3500 m to be stably stratified. While both the sounding data and upper-air maps show cold air advection associated with the system, the sequence of soundings shows that this preflight cooling extended throughout the troposphere, resulting in only a few thin regions of conditional instability. The soundings also show dewpoint temperatures to be largely within 2°–4°C of saturation at levels between several hundred meters above the surface to the base of an overlying drier air mass, which descends with time.

From a sounding (2155 UTC) performed shortly after the start of flight observations over the Park Range, vertically propagating waves were supported for wavelengths >1 km over the altitude range 2900–3500 m, and for wavelengths >3 km over the altitude range 3500–5400 m. Additionally, in this upper layer, which encompassed the in situ observations from the UWKA, the criteria for wave trapping were met for wavelengths from 3 to 9 km. For the 0108 UTC sounding, roughly 100 min after the completion of Park Range transects, vertical wave propagation was supported from the mountain peak up to flight level for wavelengths >4.4 km, and wave trapping criteria were met for wavelengths from 4 to 63 km. The horizontal forcing scale of the Park Range is about 15–18 km.

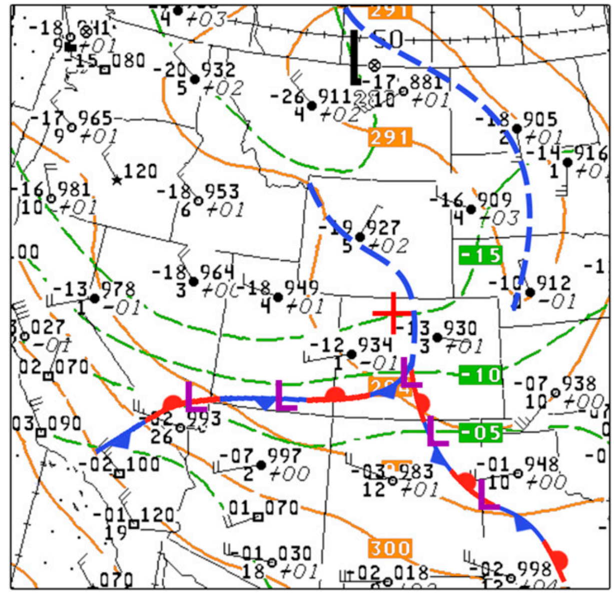

FIG. 4. Synoptic environment over western United States for flight on 9 Jan 2011 (reanalysis valid at 0000 UTC 10 Jan) showing geopotential height (solid orange contours) and temperature at 700 hPa (dashed green contours) from NCEP reanalysis. Also shown is the approximate location of surface fronts, based on the NWS surface analysis for 0000 UTC 10 Jan. A red cross symbol marks the location of Steamboat Springs, CO.

The UWKA flight track was oriented on a west-southwest line that passed over SPL and that was located ~3.8 km south of the valley floor site at closest approach (Fig. 1). Based on nine transects, a composite profile of vertical winds across the ridge axis (Fig. 6) shows bin-mean vertical winds ranging from −1.2 to 1.1 m s^{-1}, with a mean standard deviation of 0.43 m s^{-1}. A lee downdraft, centered 4–6 km downwind from the ridge axis, appears in the majority of transects from this day, and has a mean vertical velocity of −1.2 m s^{-1}. These observations, made roughly 1000 m above the ridgetop, likely show a vertically propagating mountain wave, as suggested by the radiosonde analysis. Farther downwind in the ridge lee, all transects show a roughly similar pattern of vertical wind oscillations. These oscillations have a mean horizontal wavelength of ~9.7 km ($\sigma = 1.1$ km, $n = 9$); this is near the theoretically trapped wavelengths from either bracketing sounding. Both radar and lidar profiles (Fig. 7) show signatures of this lee-wave pattern downstream of the ridge axis.

Liquid-water-containing cloud regions at flight level were most abundant upwind from the ridgeline (3–14 km), above the steepest windward topography of the Park Range. In all transects, the liquid-containing areas partially overlapped with a zone of upward vertical velocities, with the liquid regions usually offset several kilometers downwind from the region of upward air

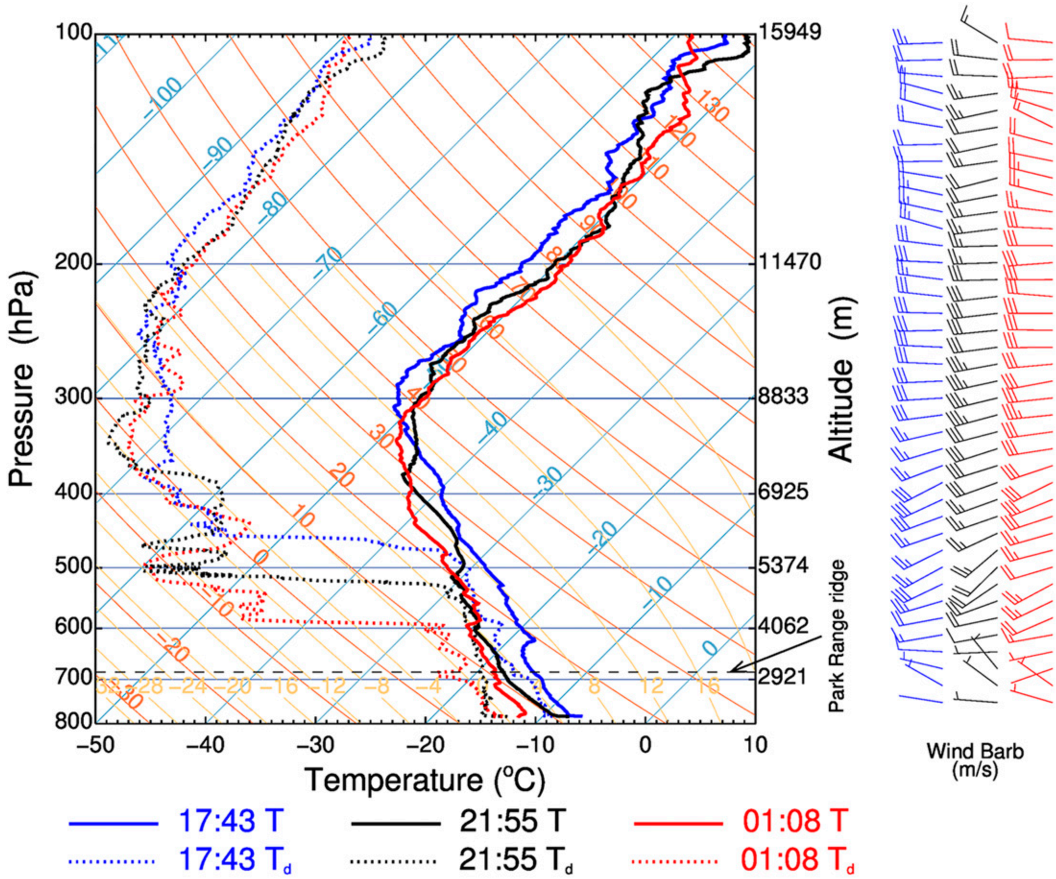

FIG. 5. Upper-air conditions above Yampa Valley at 1743 and 2155 UTC 9 Jan 2011 and 0108 UTC 10 Jan 2011, as observed with radiosondes released from the valley floor site. Measured altitudes are from the sounding at 2155 UTC. The Park Range ridge height (3092 m), calculated as the maximum of the meridional-average topography profile, is indicated with a dashed line. All times are in UTC.

motion. In a few instances, liquid water was found embedded in ice clouds at locations distant from the ridge, including at the upwind boundary of the study area and in the crests of downwind trapped lee waves. While these clouds located farther from the ridge had relatively less LWC, the RID confirmed the presence of supercooled liquid water and the FSSP showed a liquid-droplet-sized mode with particles between 4 and 20 μm. The remote sensing observations also show liquid-bearing clouds to exist within several hundred meters of the ridgetop, where increased radar reflectivities, and likely snowfall rates, are observed.

5. Composite analysis

The previous section demonstrates that individual across-ridge transects during the same storm have both significant interleg variability and some important commonalities in air motion and microphysical features. Because the CAMPS operations spanned multiple storms and several months, the resulting observations allow us to assess interstorm variability. This perspective offers information about the prevailing structures common over multiple storms and the representativeness of specific features that may appear within individual flight days. To focus on westerly flow over the Park Range, flights were only included in this analysis if winds were from the west and aircraft transects fell along a roughly E–W axis (±45°). A total of 10 of the research flights, listed in Table 1, met these qualifications and are considered in this composite analysis.

Among observations (n = 29 024) from transects that meet the criteria, the phase-determination algorithm finds that 73.0% of in-cloud regions were identified as ice only and 25.8% as mixed phase. Liquid-only regions accounted for 1.2% of the observations. Figure 8 shows the fraction of in-cloud observations identified as mixed phase or liquid only, binned by E–W location relative to the mean ridge axis. Mixed-phase fraction generally increases with approach toward the ridge axis from the

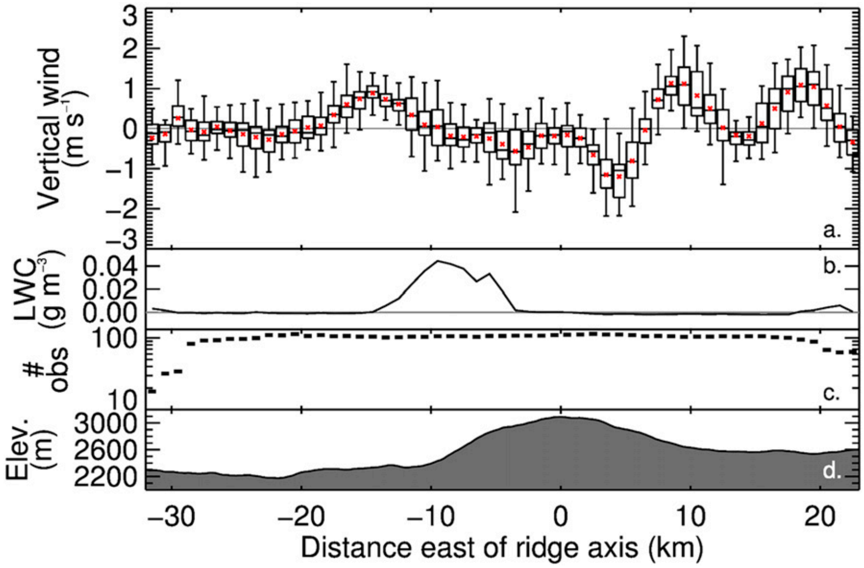

FIG. 6. Vertical wind statistics (a) shown as a function of E–W distance from mean ridge axis for 9 transects at 4200 m performed on 9 Jan 2011. Observations are grouped into 1-km-wide E–W bins. The boxes show the interquartile range (IQR), the horizontal line in the box is the median, and the whiskers show the 5th and 95th percentiles, while the red symbol is the mean. Also shown are (b) the meridionally averaged LWC measured with the PVM, (c) the number of observations in each bin, and (d) the meridional mean surface elevation.

west, reaching a peak of 43.8% at 5.5 km west from the ridge. Passing over the ridge axis and into the lee, the mixed-phase fraction decreases toward a minimum of 10.4% at 13.5 km east from the ridge. This reduction in mixed-phase fraction is likely related to the frequent occurrence of leeside subsidence, and resulting adiabatic warming and evaporation of liquid water. The relatively few liquid-only observations are clustered above the windward slopes and ridgeline of the Park Range, with another cluster in the ridge lee. The overall number of observations identified as in-cloud increases in the area upwind from and directly above the ridge. The observed spatial distribution of mixed-phase regions coincides well with numerical modeling results for cold clouds over the Park Range (Saleeby et al. 2009, 2013), suggesting that some models are capable of representing the necessary growth and dissipation processes. If only relatively dense clouds with CWC $\geq$ 0.1 g m^{-3} are considered (n = 11 066), mixed-phase clouds represent 57.4% of the observations—an increased fraction—with ice-only clouds accounting for 40.9% and liquid-only clouds accounting for 1.7%. The mixed-phase fraction peaks at 83.1%; this maximum remains located in the bin centered 5.5 km west of the ridge axis. Among low-CWC clouds (0.005 $\leq$ CWC $\leq$ 0.1 g m^{-3}), 92.8% are ice only; this results in an increase in mixed-phase fraction when only dense clouds are considered.

Vertical winds have an important effect on cloud water phase through adiabatic temperature changes and water transport. The distributions of vertical wind speeds for all cross-ridge transects (Fig. 8) illustrate the transition in airflow in the proximity of the Park Range. Considerable variability exists in bins at all locations. Both mixed-phase and ice-only observations exhibit a median pattern of small upward vertical velocities windward of the ridge and greater-magnitude descent in the ridge lee. However, several phase-specific differences are observed. The mean vertical winds are found to be significantly (at 99% confidence) more upward in mixed-phase than in ice-only regions upwind from the ridge axis. This upward motion may reflect the convective ascent of a saturated air mass, or may reflect the stronger vertical velocities needed to sustain a mixed-phase cloud, as liquid water is lost through the Wegener–Bergeron–Findeisen process (WBF). The location of maximum upward wind velocity is ~5 km west of the location of maximum mixed-phase cloud fraction, suggesting a cloud growth time scale of several minutes. Case-by-case inspection suggests the presence of a leeside mountain wave, often with just a single crest (Durran 1990), in 8 out of 10 of the flight days; these waves vary in wavelength, lee-relative position, and vertical wind magnitude. This results in increased leeside variability in the composite statistics, especially when mixed-phase clouds occur, while less variability is

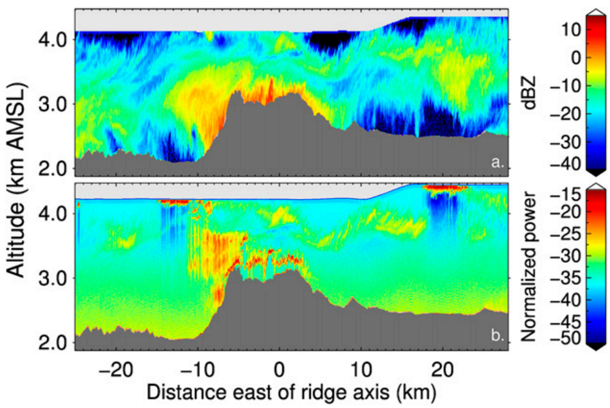

FIG. 7. Observations over the Park Range of (a) equivalent radar reflectivity (dBZ) and (b) normalized lidar backscatter power for a single transect starting at 2319 UTC 9 Jan 2011. Regions of strong lidar backscatter indicate the likely presence of liquid-water cloud. Lidar observations were smoothed with a 4.5-m boxcar average. Radar and lidar data above flight level are masked in light gray, and the terrain is masked in dark gray.

observed among the measurements for most individual days. Because of this greater variability, many of the leeside bins have statistically similar phase-specific mean vertical wind speeds. Of those lee bins found to have statistically different means, equal numbers show greater mean ascent in mixed-phase regions and in ice-only regions.

The mean vertical wind speed for all data in mixed-phase regions is 0.09 m s^{-1} (median = 0.13 m s^{-1}, n = 7501), significantly greater than the mean speed of -0.05 m s^{-1} in ice-only regions (median = -0.01 m s^{-1}, n = 21 185). A Student's t test rejects the null hypothesis that the mean vertical wind in mixed-phase regions is equal to or less than zero at the 99% confidence level. Variability in the vertical wind speeds, evaluated as the standard deviation, is also greater in mixed-phase regions (0.92 m s^{-1}) than in ice-only regions (0.63 m s^{-1}). In nearly all bins, a wider range of winds at the 95th percentile is found for mixed-phase than for ice-only regions. Though not shown, in cloud-free regions, the magnitude of the mean vertical wind is 0.01 m s^{-1} (n = 25 784) and has a standard deviation of 0.83 m s^{-1}, which is between that for ice and mixed-phase clouds. An F test for equality of variances indicates that a statistically significant (n = 47 891) greater vertical wind variance is found in cloud-free regions compared to in ice-cloud regions, though it is unclear why this behavior exists. The large positive and negative vertical velocities in mixed-phase clouds, indicated by the larger standard deviation in these clouds, reflects the tendency for liquid-containing clouds to occur in regions of unstable or turbulent air motion, or where strong upward and downward orographic forcing is occurring.

Because liquid-water clouds tend to be composed of large concentrations of small particles, the spatial distribution of small particles offers a means of comparing liquid-water location among flight days. Manual inspection of the RID observations confirms that supercooled liquid water is present in most locations where small particles are concentrated. The small-particle size distributions from the FSSP (before 15 January 2011) and the CDP (after that date) are averaged within bins by E–W location, producing transects of mean small-particle size distribution for each flight (Fig. 9). A particle-shattering signature appears in the FSSP measurements as a weak, spatially uniform mode with $D >$ 12 μm.

The location of cloud-droplet-sized particles varies substantially between flights. On all days where lee downdrafts are observed (15 December 2010, 9 January, 19 January, 22 January, 24 February, and 27 February 2011), liquid-droplet-sized particles were recorded upwind of the ridge axis but diminished in number in the ridge lee. A contrast can be drawn with observations on 16 February and 26 February 2011. On these days, mountain-scale gravity waves were absent at flight level, likely due to the neutral stability profiles observed. Unlike conditions on most flight days, cloud-droplet-sized particles were initially encountered just upwind of the topographic barrier and extend beyond the ridge lee. A further distinct scenario is observed on the two days in which the sounding stability analysis suggested that barrier-scale trapped lee wave trains were supported at flight level (9 January and 27 February 2011). On these dates, a narrow, concentrated region of small particles appears downwind from the ridge lee, amid air rebounding upward after being displaced in the lee downdraft. A similar small-particle feature, observed downwind from the ridgeline on 15 December 2010, may result from partial trapping of wave energy (KPHS).

The location and number concentration of ice particles also has an important role in controlling the evolution of the precipitation and water phase of a cloud system. Glaciation rate is a function of ice particle number concentration (Korolev and Isaac 2003), as riming and deposition processes may deplete supercooled liquid water. Mean large-particle number concentrations ($D >$ 100 μm) are found to increase in the vicinity of the ridge (Fig. 10), and are greater (at 99% confidence) in ice-only clouds than in mixed-phase clouds. However, on average, particles larger than 700 μm are more abundant in mixed-phase regions. This may result from ice particles more efficiently growing to large sizes—or adopting denser graupel-like habits—and falling out from mixed-phase clouds, or could reflect the rapid glaciation of mixed-phase clouds in the

TABLE 1. Summary of research flights included in analysis.

Flight ID	Flight date[a]	Flight time (UTC)	Mean wind direction[b] (°)	Mean wind speed[b] ($m\,s^{-1}$)	Flight altitude (m MSL)	Synoptic note
RF 1	15 Dec 2010	1644–1917	260	23.9	4600, 5300, 6100	Frontal zone
RF 2	20 Dec 2010	2259–0200	250	39.7	4900–7000, 7900	Post–cold front
RF 5	9 Jan 2011	2131–2327	245	20.1	4200	Post–cold front
RF 9	19 Jan 2011	1649–1845	280	20.5	4300, 5200, 6100	Frontal zone
RF 12	22 Jan 2011	1657–1901	295	19.9	4300, 5700	Post–cold front
RF 14	31 Jan 2011	1903–2141	275	13.1	4300–5100, 6600	Stationary front to east
RF 21	16 Feb 2011	1935–2144	250	32.5	4600, 5200–6700	Frontal zone
RF 26	24 Feb 2011	1816–1936	260	18.7	4500, 5100	Stationary front to east
RF 28	26 Feb 2011	1815–1954	255	24.5	4500, 4800, 5200	Frontal zone
RF 29	27 Feb 2011	1819–2036	275	13.8	4700, 5200, 6600	Post–cold front

[a] UTC date at flight start.
[b] Wind speed and direction are vector means of north and east components over all transects.

presence of high concentrations of ice particles (e.g., Korolev and Isaac 2003).

To examine spatial variations in ice particle concentration, observations from the region farthest upwind in the study area (22–32 km west of the ridge) are compared with observations from the region immediately upwind from the ridge (0–10 km west of the ridge). In ice-only clouds, the mean large-particle number concentration increases from $10.9\,L^{-1}$ ($\sigma = 10.0\,L^{-1}$; $n = 2989$) to $15.4\,L^{-1}$ ($\sigma = 12.1\,L^{-1}$; $n = 4104$), or 41%, from the farthest-upwind region to the near-ridge region. In mixed-phase clouds, the mean large-particle number concentration increases from $4.6\,L^{-1}$ ($\sigma = 10.8\,L^{-1}$; $n = 839$) to $5.6\,L^{-1}$ ($\sigma = 7.0\,L^{-1}$; $n = 2504$), or 22% with approach to the ridge. Both are significant increases at the 99% confidence level.

The decrease in ice particle concentrations in the lee may reflect both actual changes in cloud composition, such as that due to particles sublimating or falling out, and apparent changes due to the downward advection of clouds while sampling at a fixed altitude. On some days, radar profiles from the UWKA show cloud-top heights to decrease in the ridge lee (e.g., Fig. 7); as a result, the flight-level measurements made through the cloud are from a less-dense upper portion of the cloud, although a greater-reflectivity region persists at lower altitudes. In contrast, radar observations at other times show nearly cloud-free conditions to extend to the ground in the ridge lee; in these scenarios, low ice particle number concentrations observed at flight level are more representative of the air column to the surface. On some flight days (20 December 2010, 19 January, and 31 January 2011) ice clouds extend throughout the study area and may only be slightly reduced in the ridge lee; these days also exhibit the least overall amount of liquid water. However, there are several days (9 January, 22 January, 24 February, and 27 February 2011) in which a large reduction in large-particle number concentrations results in very little ice cloud beyond the ridge lee. As was the case for cloud-droplet-sized particles, contrasting observations are found on the dates with neutral atmospheric stability profiles and only very weak lee subsidence: 16 February and 26 February 2011. On these dates, large-particle concentrations peak in the ridge lee.

Significantly greater mean CWC is observed in mixed-phase (mean = $0.090\,g\,m^{-3}$; $\sigma = 0.071\,g\,m^{-3}$; $n = 7501$) than ice-only regions ($0.029\,g\,m^{-3}$; $\sigma = 0.044\,g\,m^{-3}$; $n = 21\,185$) over much of the study area (Fig. 11). Considering spatial changes within the phase categories, a significant increase in mean CWC over the ridge axis is observed for both mixed-phase and ice-only clouds. Using the same upwind and near-ridge 10-km comparison regions as for the large-particle number concentrations, the mean ice-only CWC increases 25%, while the mean mixed-phase CWC increases 109% from the farthest-upwind region to the near-ridge region. The increase in mixed-phase CWC extends from the ridge to nearly the downwind boundary of the study area with a lot of variability.

6. Discussion

Though considerable variability in vertical winds is observed between storms over the Park Range, the composite vertical wind pattern resembles the theoretical streamlines for steady, stable airflow over an isolated ridge (Durran 1990). Vertical ascent is favored windward of the mountain ridge, and many of the flight days exhibit a strong lee downdraft. The CAMPS observations encompass not only periods of stable air passage over the barrier, but also the combined effect of individual convective cells triggered by orographic ascent, of turbulence caused by the elevated terrain, and of shallow convection triggered by frontal forcing.

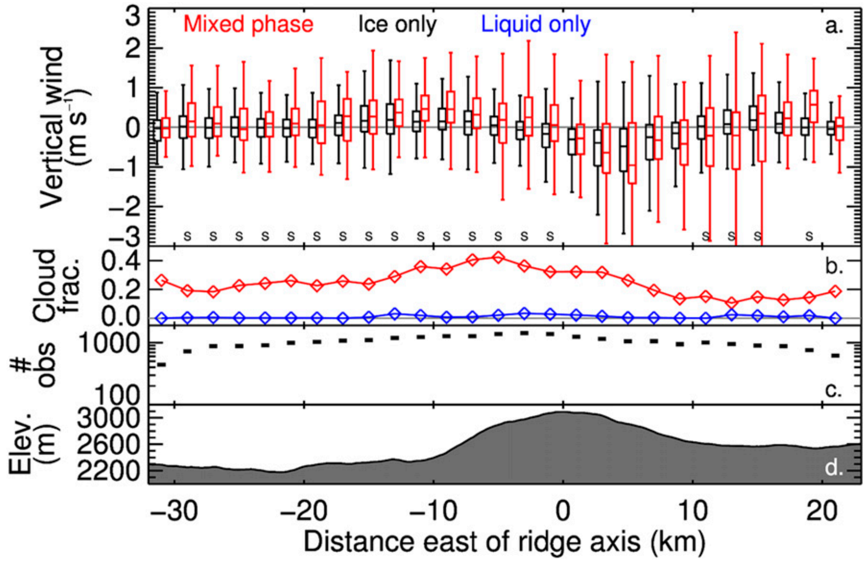

FIG. 8. Composite analysis showing (a) vertical wind speed statistics, combined for all flight days, for mixed-phase and ice-only clouds. Liquid-only clouds are not shown because of the small sample size. Observations are divided by cloud phase in 2-km-wide E–W bins. The boxes show the interquartile range (IQR), the horizontal line in the box is the median, and the whiskers show the 5th and 95th percentiles. Where the mixed-phase and ice-only means are found to be statistically different at 99% confidence using a Student's *t* test, the bins are labeled with an ''S.'' Also shown are (b) the fraction of in-cloud observations identified as mixed phase and liquid only with the remaining fraction of observations being ice only, (c) the number of in-cloud observations in each bin, and (d) the meridional mean surface elevation.

Variability in the vertical wind (Fig. 8) increases downwind from the barrier, in part because the composite analysis contains observations from days with different trapping conditions, including observations of large magnitude vertical winds in trapped lee waves on 9 January and 27 February 2011. Vertical winds were more variable and significantly more upward in mixed-phase regions than in ice-only regions.

Vertical air motion associated with mountain waves appears to be an important factor in the distribution of liquid-water clouds. Lee downdrafts have the potential to influence cloud development, as adiabatic warming in descending clouds in the ridge lee will decrease supersaturation, and suppress production of liquid water or induce evaporation. Additionally, vertical displacement of the air mass in a lee downdraft reduces cloud-top heights. These processes are likely involved in the reduced flight-level number concentration of liquid-droplet-sized particles (Fig. 9) found downwind from the ridge axis on those days in which flight-level lee downdrafts are observed. Borys et al. (2000) schematize this leeside subsidence and evaporation. Additionally, liquid water was encountered in rebounding air downwind from the ridge lee on those days that trapped lee waves were supported at flight level. These observations illustrate one aspect of the relationship between mountain wave structure and the location of liquid water within larger mixed-phase systems, and this ridge-relative displacement of liquid-water regions could have important implications for the extent of cloud cover or associated precipitation.

Mixed-phase clouds are not limited to the near-ridge region (Fig. 8), but appear throughout the 55-km-wide study area. Regional topography, which slopes upward from the west (Fig. 2), may be responsible for inducing more widespread ascent. Additionally, blocking of stable air by terrain can extend the region of orographic ascent in the upwind direction (Watson and Lane 2012). However, processes besides terrain-forced ascent may also support mixed-phase conditions in these regions. Among the nonorographic processes that may be responsible for producing mixed-phase clouds elsewhere in the study area are frontal lifting (Matejka et al. 1980; Field et al. 2004), active embedded convection (Hogan et al. 2002), or the mechanisms proposed for longer-term persistence of mixed-phase clouds, such as cloud-top radiative cooling (Pinto 1998) and turbulent or oscillatory air motion (Korolev and Field 2008). Observations at the upwind edge of the study area may provide a reference for the regional atmospheric conditions, including frontally forced convection or other dynamic effects, absent a topographic barrier. In their case study

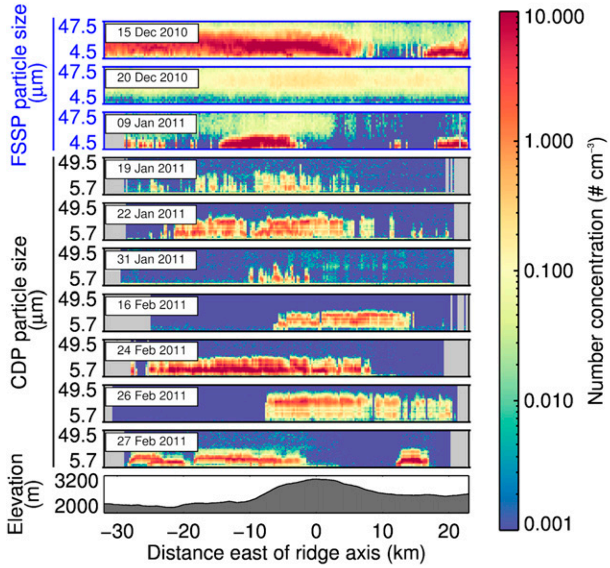

FIG. 9. Composite profiles of small-particle size distribution observed across the Park Range for 10 flight days. Observations are from FSSP for flights before 15 Jan 2011 (blue axes), and from CDP for flights after that date (black axes); size axes are linear and cover the full range of instrument bin sizes. Bins with less than 15 observations are masked in gray. Shown at bottom is the meridional mean surface elevation.

focusing on the 15 December 2010 storm over the Park Range, KPHS show that a region of enhanced radar reflectivity exists just above an elevated vertical shear layer that extends from ~25 km upwind of the ridge axis to slightly in the lee. They suggest that turbulence in this layer may be a factor in enhancing precipitation growth.

It is of scientific interest to compare the overall incidence of cloud-phase types during CAMPS (25.8% mixed phase, 1.2% liquid only) with that found in other studies, including those focused on low-topography and Arctic environments. Three autumn and winter research flights through frontal clouds at high altitudes over modest topography reported by Field et al. (2004) found no mixed-phase clouds at the same temperature range as the CAMPS data (−25° to −15°C) with one technique, while identifying mixed-phase clouds 52% of the time with another. This higher percentage is more consistent with those found by other studies (e.g., Bower et al. 1996; Korolev et al. 2003), in which mixed-phase cloud percentages of 10%–60% are reported for this temperature range. At slightly warmer temperatures (−15° to −4°C), Field et al. (2004) did find mixed-phase cloud fractions of 3%–19%, with the first technique and 30%–50% with the second. These mixed-phase cloud fractions at the slightly warmer temperatures are consistent with other nonorographic studies summarized in Field et al. (2004) and elsewhere (e.g., Matejka et al. 1980). In the Arctic, mixed-phase clouds, typically stratocumulus clouds, can persist for several days, exist 25%–47% of the time depending on location, and are the most prevalent cloud type for temperatures between −5° and −15°C (Shupe 2011). Hence, the mixed-phase cloud fraction observed during CAMPS is in the range found for frontal clouds and low-topography clouds, though it may be larger than previously found for the very limited observations reported within the CAMPS temperature range. However, the comparisons are complicated by the divergent environments in which, and mechanisms by which, mixed-phase clouds form. Also, because sampling during CAMPS targeted times in which mixed-phase clouds were expected to be present, the overall incidence of mixed-phase clouds may be biased high.

The CWC generally increases along the windward slope of the Park Range, with the greatest median CWC values observed 4 km leeward of the ridge axis. While the near-ridge increase in CWC likely reflects the flux of condensate in updrafts, the displacement of the peak CWC downwind from the region of strongest orographic ascent may reflect the downwind advection of growing convective cells triggered near the barrier. Furthermore, significantly greater CWC is found in mixed-phase regions than in ice-only regions. Efficient glaciation mechanisms limit the lifetime of mixed-phase regions, or constrain their location to environments where they are sustained by a condensate supply, such as in updrafts; this is evidenced in the present study by greater net upward motion and increased vertical wind variability where mixed-phase clouds are present. CWC may be greater in these regions of active condensate production, as recently generated particles will have had little time to fall out. While median CWCs are greater in mixed-phase clouds, greater median number concentrations of large, ice-sized particles are observed in the absence of liquid water. This situation could arise if efficient particle growth through riming or deposition in mixed-phase regions, and resulting greater ice particle fall speeds (Mitchell 1996), caused more particles to fall out from the air mass. A similar preferential depletion of ice crystals within liquid-bearing regions is observed in mixed-phase cloud tops in the Arctic (McFarquhar et al. 2007).

Cloud-top liquid layers were observed during several flights. The cloud-top water phase is particularly important in determining the cloud net radiative effect (Shupe and Intrieri 2004), but also may influence the stability and evolution of the air mass itself, as has been observed in the Arctic (e.g., Pinto 1998). In a mountainous, midlatitude region such as the Park Range, the powerful mechanisms of orographically forced ascent, the release of convective instability, and terrain-induced turbulence (Geerts et al. 2011) are likely dominant drivers for condensate production. However, the radiative

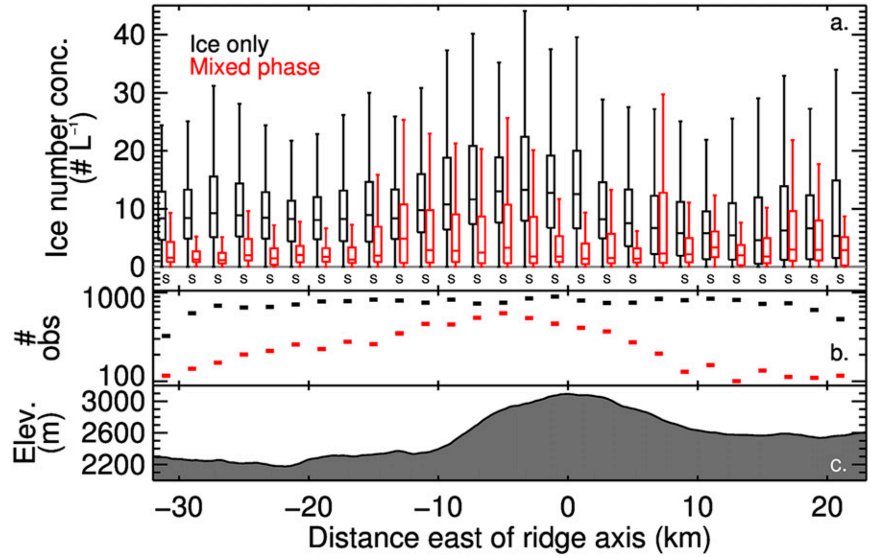

FIG. 10. (a) Composite analysis as in Fig. 8, but showing statistics for number concentration of ice-sized cloud particles ($D > 100\,\mu$m) observed with the 2DC probe. Also shown are (b) the number of observations in ice-only and mixed-phase clouds for each bin and (c) the meridional mean surface elevation.

properties of the cloud-top liquid may play a role in supporting further condensate production, particularly as the evolving air mass is advected beyond the region of strongest orographic ascent.

In at least five transects from 9 January 2011, the downward-facing lidar observations show the ridge to be capped with a thin liquid cloud layer (e.g., Fig. 7), as identified by both the high power and low depolarization ratios of the lidar backscatter. The interpretation that some combination of ice particle riming or enhanced depositional growth is occurring in this region is supported by the large increase in radar reflectivity below the low-level liquid clouds, which suggests ice crystal growth and a significant increase in particle size within several hundred meters of the mountaintop. Previous oxygen isotopic analysis of snowfall at this site suggested that low-altitude cloud growth was substantial, with Lowenthal et al. (2011) determining that the mass-weighted altitude of snow growth was <300 m above the ridge. Furthermore, that this liquid-containing region is found so close to the surface allows for the possibility that the mixed-phase conditions were supported by the intersection of the turbulent boundary layer with the cloud base, a mechanism described by Geerts et al. (2011). This configuration is further suggested by the intensification of the near-surface backscatter at roughly the altitude at which the rising terrain meets the apparent cloud base in the lidar profiles. The large snow mass fraction attributable to low-altitude riming may reflect not only an enhancement of particle mass by riming, but also the preferential precipitation of rimed particles, in which case a cloud-top liquid cap could alter whether precipitation occurred at all (Reinking and Snider 2000). Further insights could be provided by using Doppler analysis to determine the depth of the turbulent boundary layer (Geerts et al. 2011; KPHS) in relationship to the liquid-water extent, particularly in those locations where the top of the liquid layer reaches its greatest elevation above the terrain. Also significant is that this near-surface liquid-water region is not limited to the windward slopes and ridges, but extends downwind for ~10 km, enlarging the region over which liquid-related ice-particle growth processes, such as riming and WBF deposition, can occur. Numerical model results (Saleeby et al. 2009, 2013) show significant accumulation to occur on the lee slopes of the Park Range, as wind-borne precipitation is carried over the ridge; liquid-water clouds in the ridge lee could augment the precipitated water mass in these regions. Near-surface liquid-water lidar signatures were also observed on other days during the campaign, and previous observations showed the frequent presence of mountaintop-level liquid water in the Park Range (Hindman 1986).

In their analysis of the 15 December 2010 storm over the Park Range, KPHS assess temporal and along-ridge spatial variations in storm structure. These are relevant to the interpretation of the composite observations presented here, as they reflect on the assumptions made in producing composite profiles that include flight legs from multiple locations along the Park Range, and that

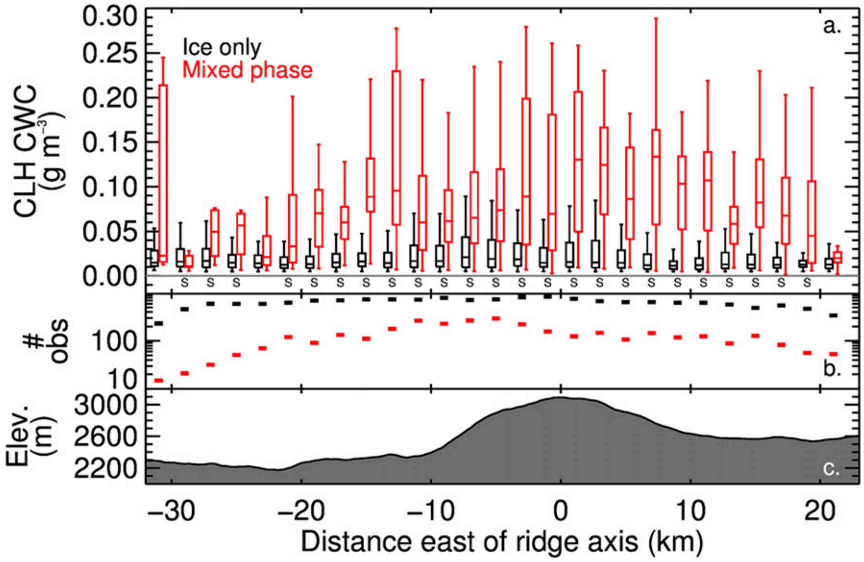

FIG. 11. As in Fig. 8, but showing (a) cloud water content (CWC).

include observations often made over the course of several hours during individual storms. KPHS found that wind fields and radar reflectivity patterns did evolve over the course of the 2.5-h flight, while a mountain wave and trapped lee wave structure persisted, and that peak radar reflectivity and cloud-top heights varied with north–south location along the ridge.

This study focuses on storms over a single mountain barrier, the Park Range, which is among the primary upwind barriers for westerly flow over the mountains of Colorado, and which has been shown to experience mountaintop-level supercooled liquid-water events more frequently than downwind topographic barriers (Hindman 1986). This effect may be caused by the precipitation of water mass over the primary barriers and the resulting reduced total water content (TWC) downwind, or by the impact of the primary barrier on downstream airflow and disruption of orographic lifting. The observations over the Park Range may therefore reflect a greater incidence of supercooled liquid water than is experienced by more-protected mountain barriers elsewhere in the southern Rockies. However, other primary topographic barriers may experience a yet-greater incidence of supercooled liquid water, as is the case for the San Juan Mountains in southern Colorado (Saleeby et al. 2011).

7. Conclusions

The CAMPS aircraft campaign targeted observations of mixed-phase clouds and precipitation in an orographic environment during the 2010/11 winter over the Park Range in Colorado. Storms with westerly, cross-barrier winds over the range were considered; a case study from one flight and statistical composites of observations from 10 flights were presented.

The postfrontal storm examined in the case study reflected a stable air column and trapped lee waves on 9 January 2011. Remote sensing observations both of a near-ridgetop mixed-phase region embedded in a larger ice cloud, and of a collocated increase in radar returns that suggests ice particle growth, bolster existing isotopic (Lowenthal et al. 2011) and Doppler radar evidence (Geerts et al. 2011) for the role of near-surface mixed-phase processes in modifying precipitation.

Multiday across-ridge composites show transitions in vertical wind, cloud water phase, and other microphysical characteristics in the approach and passage of air over the western ridge of the Park Range. In the composites, a peak in mixed-phase cloud frequency is located approximately 5 km downwind of a peak in median vertical air motion windward of the ridge axis (Fig. 8); the frequency of mixed-phase clouds decreases sharply as median vertical wind becomes negative near the ridge axis. On many flight days, a similar pattern of near-ridge liquid-containing regions is suggested by the presence of cloud-droplet-sized particles (Fig. 9), with concentrations again reduced in the ridge lee. However, cloud-droplet-sized particles are still observed in some convective cells, in the crests of lee waves (9 January), and on some days with weak or no mountain waves. Leeside reductions in the CWC, in the number concentration of ice-sized particles and in the mixed-phase cloud fraction indicate a shift in this region toward particle loss mechanisms of evaporation and fallout. Lee downdrafts and resulting adiabatic warming likely contribute to this process.

While precipitated snow mass generally increases toward the windward slope of the Park Range (Saleeby et al. 2009), observations from two days (16 February and 26 February 2011) showed liquid water regions and strong updrafts beyond the ridge lee; these days also exhibited neutral stability profiles and the absence of flight-level lee downdrafts. Determining the downwind extent of these lee-oriented storms and their potential for precipitation production could provide significant insights into the distribution of snowfall across a barrier. Such information is of paramount importance to water resource planners, since mountain ridges also partition snowmelt into drainage basins.

Acknowledgments. The Colorado Airborne Multiphase Cloud Study (CAMPS) was sponsored by the National Science Foundation (NSF) under Grant AGS-0964238. M. S. was additionally supported by the U.S. Department of Energy (DOE) Atmospheric System Research Program Grant DE-SC0011918. The authors thank the StormVEx and CAMPS science teams for planning and directing these projects, and are deeply grateful to the staff and crew of the University of Wyoming King Air for conducting the airborne observations and to Zhien Wang for providing support with aircraft remote sensor measurements. Radiosonde data were provided by the U.S. DOE Atmospheric Radiation Measurement Program. This manuscript was written while the first author was a visiting research fellow at the Institute for Climate and Atmospheric Science, University of Leeds, United Kingdom.

REFERENCES

Baumgardner, D., 1983: An analysis and comparison of five water droplet measuring instruments. *J. Climate Appl. Meteor.*, **22**, 891–910, doi:10.1175/1520-0450(1983)022<0891:AAACOF>2.0.CO;2.

——, and A. Rodi, 1989: Laboratory and wind-tunnel evaluations of the Rosemount icing detector. *J. Atmos. Oceanic Technol.*, **6**, 971–979, doi:10.1175/1520-0426(1989)006<0971:LAWTEO>2.0.CO;2.

——, H. Jonsson, W. Dawson, D. O'Connor, and R. Newton, 2001: The cloud, aerosol and precipitation spectrometer: A new instrument for cloud investigations. *Atmos. Res.*, **59–60**, 251–264, doi:10.1016/S0169-8095(01)00119-3.

Bergeron, T., 1949: The problem of artificial control of rainfall on the globe: I. General effects of ice-nuclei in clouds. *Tellus*, **1A**, 32–43, doi:10.1111/j.2153-3490.1949.tb01926.x.

Borys, R. D., and M. A. Wetzel, 1997: Storm Peak Laboratory: A research, teaching, and service facility for the atmospheric sciences. *Bull. Amer. Meteor. Soc.*, **78**, 2115–2123, doi:10.1175/1520-0477(1997)078<2115:SPLART>2.0.CO;2.

——, D. H. Lowenthal, and D. L. Mitchell, 2000: The relationships among cloud microphysics, chemistry, and precipitation rate in cold mountain clouds. *Atmos. Environ.*, **34**, 2593–2602, doi:10.1016/S1352-2310(99)00492-6.

Bower, K. N., S. J. Moss, D. W. Johnson, T. W. Choularton, J. Latham, P. R. A. Brown, A. M. Blyth, and J. Cardwell, 1996: A parameterization of ice water content observed in frontal and convective clouds. *Quart. J. Roy. Meteor. Soc.*, **122**, 1815–1844, doi:10.1002/qj.49712253605.

Carey, L. D., J. Niu, P. Yang, J. A. Kankiewicz, V. E. Larson, and T. H. V. Haar, 2008: The vertical profile of liquid and ice water content in midlatitude mixed-phase altocumulus clouds. *J. Appl. Meteor. Climatol.*, **47**, 2487–2495, doi:10.1175/2008JAMC1885.1.

Cober, S. G., G. A. Isaac, and A. V. Korolev, 2001: Assessing the Rosemount Icing Detector with in situ measurements. *J. Atmos. Oceanic Technol.*, **18**, 515–528, doi:10.1175/1520-0426(2001)018<0515:ATRIDW>2.0.CO;2.

Cotton, R., S. Osborne, Z. Ulanowski, E. Hirst, P. H. Kaye, and R. S. Greenaway, 2010: The ability of the Small Ice Detector (SID-2) to characterize cloud particle and aerosol morphologies obtained during flights of the FAAM BAe-146 research aircraft. *J. Atmos. Oceanic Technol.*, **27**, 290–303, doi:10.1175/2009JTECHA1282.1.

Davis, S. M., A. G. Hallar, L. M. Avallone, and W. Engblom, 2007: Measurement of total water with a tunable diode laser hygrometer: Inlet analysis, calibration procedure, and ice water content determination. *J. Atmos. Oceanic Technol.*, **24**, 463–475, doi:10.1175/JTECH1975.1.

Dorsi, S. W., L. E. Kalnajs, D. W. Toohey, and L. M. Avallone, 2014: A fiber-coupled laser hygrometer for airborne total water measurement. *Atmos. Meas. Tech.*, **7**, 215–223, doi:10.5194/amt-7-215-2014.

Durran, D. R., 1990: Mountain waves and downslope winds. *Atmospheric Processes over Complex Terrain, Meteor. Monogr.*, No. 45, Amer. Meteor. Soc., 59–81.

Field, P. R., R. J. Hogan, P. R. A. Brown, A. J. Illingworth, T. W. Choularton, P. H. Kaye, E. Hirst, and R. S. Greenaway, 2004: Simultaneous radar and aircraft observations of mixed-phase cloud at the 100 m scale. *Quart. J. Roy. Meteor. Soc.*, **130**, 1877–1904, doi:10.1256/qj.03.102.

Fleishauer, R. P., V. E. Larson, and T. H. Vonder Haar, 2002: Observed microphysical structure of midlevel, mixed-phase clouds. *J. Atmos. Sci.*, **59**, 1779–1804, doi:10.1175/1520-0469(2002)059<1779:OMSOMM>2.0.CO;2.

Geerts, B., Q. Miao, and Y. Yang, 2011: Boundary layer turbulence and orographic precipitation growth in cold clouds: Evidence from profiling airborne radar data. *J. Atmos. Sci.*, **68**, 2344–2365, doi:10.1175/JAS-D-10-05009.1.

Gerber, H., G. Frick, and A. Rodi, 1999: Ground-based FSSP and PVM measurements of liquid water content. *J. Atmos. Oceanic Technol.*, **16**, 1143–1149, doi:10.1175/1520-0426(1999)016<1143:GBFAPM>2.0.CO;2.

Gesch, D. B., 2007: The National Elevation Dataset. *Digital Elevation Model Technologies and Applications: The DEM Users Manual*, 2nd ed. D. Maune, Ed., American Society for Photogrammetry and Remote Sensing, 99–118.

Gordon, G. L., and J. D. Marwitz, 1984: An airborne comparison of three PMS probes. *J. Atmos. Oceanic Technol.*, **1**, 22–27, doi:10.1175/1520-0426(1984)001<0022:AACOTP>2.0.CO;2.

Gregory, D., and D. Morris, 1996: The sensitivity of climate simulations to the specification of mixed phase clouds. *Climate Dyn.*, **12**, 641–651, doi:10.1007/BF00216271.

Hallar, A. G., D. H. Lowenthal, G. Chirokova, and R. D. Borys, 2011: Persistent daily new particle formation at a mountain-top location. *Atmos. Environ.*, **45**, 4111–4115, doi:10.1016/j.atmosenv.2011.04.044.

Heggli, M. F., and R. M. Rauber, 1988: The characteristics and evolution of supercooled water in wintertime storms over the Sierra Nevada: A summary of microwave radiometric measurements taken during the Sierra Cooperative Pilot Project. *J. Appl. Meteor.*, **27**, 989–1015, doi:10.1175/1520-0450(1988)027<0989:TCAEOS>2.0.CO;2.

Hindman, E. E., 1986: Characteristics of supercooled liquid water in clouds at mountaintop sites in the Colorado Rockies. *J. Climate Appl. Meteor.*, **25**, 1271–1279, doi:10.1175/1520-0450(1986)025<1271:COSLWI>2.0.CO;2.

Hobbs, P. V., T. J. Matejka, P. H. Herzegh, J. D. Locatelli, and R. A. Houze Jr., 1980: The mesoscale and microscale structure and organization of clouds and precipitation in midlatitude cyclones. I: A case study of a cold front. *J. Atmos. Sci.*, **37**, 568–596, doi:10.1175/1520-0469(1980)037<0568:TMAMSA>2.0.CO;2.

Hogan, R. J., P. R. Field, A. J. Illingworth, R. Cotton, and T. W. Choularton, 2002: Properties of embedded convection in warm-frontal mixed-phase cloud from aircraft and polarimetric radar. *Quart. J. Roy. Meteor. Soc.*, **128**, 451–476, doi:10.1256/003590002321042054.

——, A. J. Illingworth, E. J. O'Connor, and J. Baptista, 2003a: Characteristics of mixed-phase clouds. II: A climatology from ground-based lidar. *Quart. J. Roy. Meteor. Soc.*, **129**, 2117–2134, doi:10.1256/qj.01.209.

——, P. Francis, H. Flentje, A. J. Illingworth, M. Quante, and J. Pelon, 2003b: Characteristics of mixed-phase clouds. I: Lidar, radar and aircraft observations from CLARE'98. *Quart. J. Roy. Meteor. Soc.*, **129**, 2089–2116, doi:10.1256/rj.01.208.

King, W., D. Parkin, and R. Handsworth, 1978: Hot-wire liquid water device having fully calculable response characteristics. *J. Appl. Meteor.*, **17**, 1809–1813, doi:10.1175/1520-0450(1978)017<1809:AHWLWD>2.0.CO;2.

Klein, S. A., and Coauthors, 2009: Intercomparison of model simulations of mixed-phase clouds observed during the ARM Mixed-Phase Arctic Cloud Experiment. I: Single-layer cloud. *Quart. J. Roy. Meteor. Soc.*, **135**, 979–1002, doi:10.1002/qj.416.

Korolev, A. V., and G. A. Isaac, 2003: Phase transformation of mixed-phase clouds. *Quart. J. Roy. Meteor. Soc.*, **129**, 19–38, doi:10.1256/qj.01.203.

——, and ——, 2006: Relative humidity in liquid, mixed-phase, and ice clouds. *J. Atmos. Sci.*, **63**, 2865–2880, doi:10.1175/JAS3784.1.

——, and P. R. Field, 2008: The effect of dynamics on mixed-phase clouds: Theoretical considerations. *J. Atmos. Sci.*, **65**, 66–86, doi:10.1175/2007JAS2355.1.

——, J. W. Strapp, and G. A. Isaac, 1998: Evaluation of the accuracy of PMS optical array probes. *J. Atmos. Oceanic Technol.*, **15**, 708–720, doi:10.1175/1520-0426(1998)015<0708:EOTAOP>2.0.CO;2.

——, G. A. Isaac, S. G. Cober, J. W. Strapp, and J. Hallett, 2003: Microphysical characterization of mixed-phase clouds. *Quart. J. Roy. Meteor. Soc.*, **129**, 39–65, doi:10.1256/qj.01.204.

——, E. F. Emery, J. W. Strapp, S. G. Cober, G. A. Isaac, M. Wasey, and D. Marcotte, 2011: Small ice particles in tropospheric clouds: Fact or artifact? Airborne icing instrumentation evaluation experiment. *Bull. Amer. Meteor. Soc.*, **92**, 967–973, doi:10.1175/2010BAMS3141.1.

Lance, S., C. A. Brock, D. C. Rogers, and J. A. Gordon, 2010: Water droplet calibration of the Cloud Droplet Probe (CDP) and in-flight performance in liquid, ice and mixed-phase clouds during ARCPAC. *Atmos. Meas. Tech.*, **3**, 1683–1706, doi:10.5194/amt-3-1683-2010.

Lawson, R. P., 2011: Effects of ice particles shattering on the 2D-S probe. *Atmos. Meas. Tech.*, **4**, 1361–1381, doi:10.5194/amt-4-1361-2011.

Lenschow, D., E. Miller, and R. Friesen, 1991: A three-aircraft intercomparison of two types of air motion measurement systems. *J. Atmos. Oceanic Technol.*, **8**, 41–50, doi:10.1175/1520-0426(1991)008<0041:ATAIOT>2.0.CO;2.

Lowenthal, D. H., R. D. Borys, W. R. Cotton, S. M. Saleeby, S. A. Cohn, and W. O. J. Brown, 2011: The altitude of snow growth by riming and vapor deposition in mixed-phase orographic clouds. *Atmos. Environ.*, **45**, 519–522, doi:10.1016/j.atmosenv.2010.09.061.

Matejka, T. J., R. A. Houze Jr., and P. V. Hobbs, 1980: Microphysics and dynamics of clouds associated with mesoscale rainbands in extratropical cyclones. *Quart. J. Roy. Meteor. Soc.*, **106**, 29–56, doi:10.1002/qj.49710644704.

McFarquhar, G. M., G. Zhang, M. R. Poellot, G. L. Kok, R. McCoy, T. Tooman, A. Fridlind, and A. J. Heymsfield, 2007: Ice properties of single-layer stratocumulus during the Mixed-Phase Arctic Cloud Experiment: 1. Observations. *J. Geophys. Res.*, **112**, D24201, doi:10.1029/2007JD008633.

——, J. Um, and R. Jackson, 2013: Small cloud particle shapes in mixed-phase clouds. *J. Appl. Meteor. Climatol.*, **52**, 1277–1293, doi:10.1175/JAMC-D-12-0114.1.

Mitchell, D. L., 1996: Use of mass- and area-dimensional power laws for determining precipitation particle terminal velocities. *J. Atmos. Sci.*, **53**, 1710–1723, doi:10.1175/1520-0469(1996)053<1710:UOMAAD>2.0.CO;2.

Noh, Y.-J., C. J. Seaman, T. H. Vonder Haar, and G. Liu, 2013: In situ aircraft measurements of the vertical distribution of liquid and ice water content in midlatitude mixed-phase clouds. *J. Appl. Meteor. Climatol.*, **52**, 269–279, doi:10.1175/JAMC-D-11-0202.1.

Pinto, J., 1998: Autumnal mixed-phase cloudy boundary layers in the Arctic. *J. Atmos. Sci.*, **55**, 2016–2038, doi:10.1175/1520-0469(1998)055<2016:AMPCBL>2.0.CO;2.

Rauber, R. M., 1992: Microphysical structure and evolution of a central Sierra Nevada orographic cloud system. *J. Appl. Meteor.*, **31**, 3–24, doi:10.1175/1520-0450(1992)031<0003:MSAEOA>2.0.CO;2.

——, and L. O. Grant, 1986: The characteristics and distribution of cloud water over the mountains of Northern Colorado during wintertime storms. Part II: Spatial distribution and microphysical characteristics. *J. Climate Appl. Meteor.*, **25**, 489–504, doi:10.1175/1520-0450(1986)025<0489:TCADOC>2.0.CO;2.

——, ——, D. Feng, and J. Snider, 1986: The characteristics and distribution of cloud water over the mountains of Northern Colorado during wintertime storms. Part I: Temporal variations. *J. Climate Appl. Meteor.*, **25**, 468–488, doi:10.1175/1520-0450(1986)025<0468:TCADOC>2.0.CO;2.

Reinking, R., and J. Snider, 2000: Influences of storm-embedded orographic gravity waves on cloud liquid water and precipitation. *J. Appl. Meteor. Climatol.*, **39**, 733–759, doi:10.1175/1520-0450(2000)039<0733:IOSEOG>2.0.CO;2.

Rogers, D. C., and G. Vali, 1987: Ice crystal production by mountain surfaces. *J. Climate Appl. Meteor.*, **26**, 1152–1168, doi:10.1175/1520-0450(1987)026<1152:ICPBMS>2.0.CO;2.

Rosenfeld, D., and Coauthors, 2013: The common occurrence of highly supercooled drizzle and rain near the coastal regions of the western United States. *J. Geophys. Res. Atmos.*, **118**, 9819–9833, doi:10.1002/jgrd.50529.

Saleeby, S. M., and W. R. Cotton, 2005: A large-droplet mode and prognostic number concentration of cloud droplets in the Colorado State University Regional Atmospheric Modeling System (RAMS). Part II: Sensitivity to a Colorado winter snowfall event. *J. Appl. Meteor.*, **44**, 1912–1929, doi:10.1175/JAM2312.1.

——, ——, D. H. Lowenthal, R. D. Borys, and M. A. Wetzel, 2009: Influence of cloud condensation nuclei on orographic snowfall. *J. Appl. Meteor. Climatol.*, **48**, 903–922, doi:10.1175/2008JAMC1989.1.

——, ——, and J. D. Fuller, 2011: The cumulative impact of cloud droplet nucleating aerosols on orographic snowfall in Colorado. *J. Appl. Meteor. Climatol.*, **50**, 604–625, doi:10.1175/2010JAMC2594.1.

——, ——, D. H. Lowenthal, and J. Messina, 2013: Aerosol impacts on the microphysical growth processes of orographic snowfall. *J. Appl. Meteor. Climatol.*, **52**, 834–852, doi:10.1175/JAMC-D-12-0193.1.

Shupe, M. D., 2011: Clouds at Arctic atmospheric observatories. Part II: Thermodynamic phase characteristics. *J. Appl. Meteor. Climatol.*, **50**, 645–661, doi:10.1175/2010JAMC2468.1.

——, and J. M. Intrieri, 2004: Cloud radiative forcing of the Arctic surface: The influence of cloud properties, surface albedo, and solar zenith angle. *J. Climate*, **17**, 616–628, doi:10.1175/1520-0442(2004)017<0616:CRFOTA>2.0.CO;2.

——, and Coauthors, 2008: A focus on mixed-phase clouds. *Bull. Amer. Meteor. Soc.*, **89**, 1549–1562, doi:10.1175/2008BAMS2378.1.

Wang, Z., P. Wechsler, W. Kuestner, J. French, A. Rodi, B. Glover, M. Burkhart, and D. Lukens, 2009: Wyoming Cloud Lidar: Instrument description and applications. *Opt. Express*, **17**, 13 576–13 587, doi:10.1364/OE.17.013576.

——, and Coauthors, 2012: Single aircraft integration of remote sensing and in situ sampling for the study of cloud microphysics and dynamics. *Bull. Amer. Meteor. Soc.*, **93**, 653–668, doi:10.1175/BAMS-D-11-00044.1.

Watson, C. D., and T. P. Lane, 2012: Sensitivities of orographic precipitation to terrain geometry and upstream conditions in idealized simulations. *J. Atmos. Sci.*, **69**, 1208–1231, doi:10.1175/JAS-D-11-0198.1.